NUMERICAL ANALYSIS OF THE DISTRIBUTION OF INCIDENT WAVE ENERGY ON AN ONSHORE OSCILLATING WATER COLUMN WAVE ENERGY CONVERTER

Lucas Amaral Gaspar

Paulo Roberto de Freitas Teixeira

lucas.ag92@gmail.com

pauloteixeira@furg.br

Universidade Federal do Rio Grande - FURG

Av. Itália, Km 8, 96201-900, RS, Rio Grande, Brazil

Eric Didier

Maria Graça Neves

edidier@lnec.pt

gneves@lnec.pt

Laboratório Nacional de Engenharia Civil – LNEC

Avenida do Brasil, 101, 1700-066, Lisbon, Portugal

Abstract. *In this study, a numerical analysis to evaluate the energy efficiency of an Oscillating Water Column (OWC) wave energy converter is carried out. The device geometry is based on the pilot plant installed on Pico Island, Azores, Portugal. The methodology consists in calculating the percentage of the incident energy that is distributed along the wave energy conversion. The FLUENT® numerical model, which is based on the Reynolds-Averaged Navier-Stokes (RANS) equations, is used. The Volume of Fluid (VoF) method is employed to take into account the water and air fluids. The case study comprises a flume 10 m deep with an onshore OWC at its end. The distribution of the incident wave energy (1 m wave height with a 9 s period) is determined in terms of reflected wave energy, water column oscillation potential energy, pneumatic energy and energy losses due to viscosity and turbulence dissipations. Results show that the incident wave energy is distributed around 37% for the sum of reflected wave energy and viscosity energy loss, 52% for pneumatic energy and 11% for water column oscillation potential energy.*

Keywords: *Wave energy, Oscillating Water Column device, Numerical simulation, Finite volume method, Volume of Fluid.*

1. INTRODUCTION

Over the years humans have looking for energies in the nature to develop their activities of surviving, development and recreation in unsustainable way that cause negative impacts in the environment balance. Fossil fuels are the main source, which expels large amount of gases into the atmosphere that cause greenhouse effect and other damages. Therefore, in the last years, research areas related to the sustainable development have been significantly stimulated.

Ocean energies are an alternative, presented in waves, tide currents, ocean currents, ocean thermal variabilities and salinity gradients (IPCC, 2011). Nevertheless, these types of energy sources have insignificant installed power in the global energetic matrix, differently of wind and solar energies that have developed technologies to generate electricity commercially. The main reasons of this scenario are the difficult access because of the hostile environment and the diversity of the source of the ocean energy, which cause a high cost of construction and maintenance and, consequently, promote a great challenge to design engineers. Overcome these challenges can cause a significant impact in favor of the importance of the ocean energy in the global energetic matrix, since only the available wave energy in the world is around 2 TW/year, that is similar to the world electric energy demand (Cruz, 2008). Its contribution would be significant even if only 10 to 25% of this source is extract.

Oscillating Water Column (OWC) is the wave energy converter device most studied, and consists of a concrete or steel structure (chamber) partially submerged, opened below the water free surface (Falcão, 2010). The incident wave induces an oscillation in the water level that compress and decompress the air confined inside the chamber and makes a turbine and a generator work to generate electricity (Ghosh & Prelas, 2011). This device can be floating (nearshore and offshore) or inserted in a breakwater or at the coast (onshore). Wells turbine, created in the middle of 1970, is the most used in prototypes. Its flow is axial and rotational direction is independent of flow direction. Some examples of prototypes onshore in real scale are Pico plant (400 kW) (Falcão, 2000) in Cachorro port, Azores, Portugal; LIMPET (500 kW) (Falcão, 2010) in Isley Island, United Kingdom; Toftes (500 kW), Norway; Sakata (60kW), Japan; Vizhinjam, India (Teixeira et al., 2013); Mutriku (300 kW) in Spain (Torre-Enciso et al., 2009).

Nowadays, several researchers are looking for energy wave converter devices with optimal efficiency to reach designs economically viable. However, this search requires understanding the energy balance of this complex system that involves wave-structure interaction with strong non-linearity. Therefore, since energy losses are identified and quantified, different systems can be proposed to increase the device efficiency. Tseng et al. (2000) investigated experimentally the energy balance of an onshore OWC device and reported three types of energies that could be directly identified: energy losses (mainly viscous losses), reflected energy and pneumatic energy (subdivided by effective energy and turbine losses). Folley and Whittaker (2002), reported mechanisms of the energy balance in a LIMPET-type OWC, such as run up and run down on the front wall, slosh and water oscillating inside the chamber. Elhanafi et al. (2016) numerically studied in detail the energy balance in an onshore OWC, partitioning the absorbed energy in energy losses and the water column oscillation potential energy inside the chamber. Besides, the authors employ coefficients to represent each energy quantity relative to the total one.

In this study, a numerical analysis to evaluate the energy efficiency of an OWC wave energy converter is carried out. The device geometry, based on the pilot plant installed on Pico Island, Azores, Portugal, is considered. The methodology consists in calculating the percentage of the incident energy that is distributed along the wave energy conversion. The FLUENT® numerical model, which is based on the Reynolds-Averaged Navier-Stokes (RANS) equations, discretized by means of the Finite Volume technique, is used. The Volume of Fluid (VoF) method is employed to take into account the water and air fluids. The case study comprises a flume 10 m deep with an onshore OWC at its end. An incident wave, 1 m height with a 9 s period, and a Wells turbine model are imposed by means of User Defined Functions (UDFs). The distribution of the incident wave energy is determined in terms of reflected wave energy, water column oscillation potential energy, pneumatic energy and energy losses due to viscosity and turbulence dissipations.

2. METHODOLOGY

2.1 Case study and mathematical model

The case study consists in a flume 10 m deep and with an OWC at its end (Fig. 1). The OWC chamber is 10 m wide and 10 m long with a front wall 0.5 m tick submerged in 2.5 m; the chamber height is 6 m (from the water rest level). The turbine is Wells-type with $kt = 50$ Pa s/m^3. The incident wave has a period, T = 9 s and a wave height, H = 1 m; the wavelength is $L = 81.7$ m, according to dispersion equation of a linear wave (Dean and Dalrymple, 1991). The length of the flume is 2L.

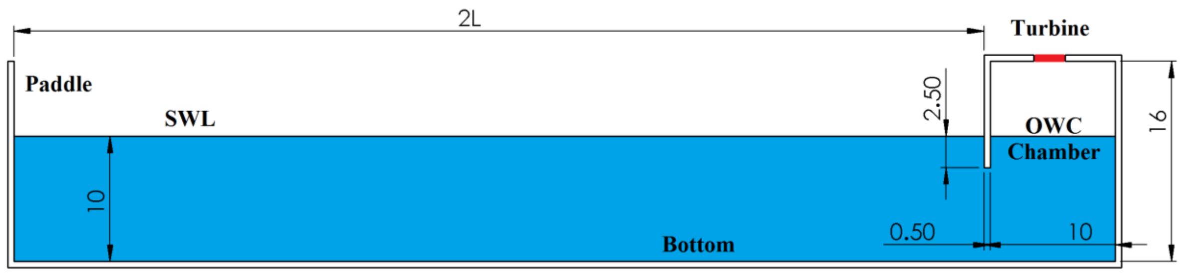

Figure 1. Sketch of the domain (dimensions in m).

Simulations are carried out by means of FLUENT® model, taking into account an incompressible fluid flow that can be described by the continuity and Navier-Stokes equations:

$$\frac{\partial u_i}{\partial x_i} = 0 \tag{1}$$

$$\frac{\partial u_i}{\partial t_i} + u_j \frac{\partial u_i}{\partial x_j} = -\frac{1}{\rho}\frac{\partial p}{\partial x_i} + g_i + \frac{1}{\rho}\frac{\partial \tau_{ij}}{\partial x_j} \tag{2}$$

where i, j =1, 2 for 2D flow and i, j =1, 2, 3 for 3D flow, u_i refers to the velocity components, t the time, p the pressure, ρ the fluid density, g_i gravitational acceleration components, and τ_{ij} the viscous stress tensor. In this study, RANS equations, based on the decomposition of the instantaneous velocity and pressure fields of the Navier–Stokes equations, Eqs. (1) and (2), into mean and fluctuating components, and the subsequent time-averaging of the set of equations, are used. This process introduces Reynolds stresses terms associated with the turbulence. A turbulence model must be introduced to relate the Reynolds stresses to mean flow variables and close the equations.

Free surface flow motion was defined by the Volume of Fluid (VOF) method which consists, through the transport equation of a scalar, the volume fraction α, (Eq. (3)) to identify the position of the free surface from the volume fraction which takes the value 0 in the air and 1 in the water. The position of the free surface is defined by the value 0.5.

$$\frac{\partial \alpha}{\partial t} + u_j \frac{\partial \alpha}{\partial x_j} = 0 \tag{3}$$

The FLUENT® model uses the finite volume method to discretize equations. In this study, the algorithm SIMPLEC (Semi-Implicit Method for Pressure Linked Equations-Consistent) to the pressure-velocity coupling and the turbulence model k-ε are used. Relaxation parameters are 0.3 for pressure, 0.7 for momentum, 1 for density, body forces and eddy viscosity, and 0.8 for turbulence kinetic energy and turbulence dissipation rate. Both phases are incompressible and the geo-reconstruct method is used to define phase interfaces. PRESTO! (PREssure STaggering Option) method is used to the spatial discretization of pressure and the interpolation scheme of third-order MUSCL (Monotone Upstream-Centered Schemes for Conservations Laws) is adopted to momentum and turbulence. The first-order implicit temporal transient formulation, with time step of 0.014 s (lower than T/600), is used.

The incident wave generation is imposed by User-Defined Function (UDF), applied on the velocity-inlet boundary (Fig. 2). Velocity component profiles, which are a function of time and depth, are imposed and the corresponding free surface position is defined by the volume fraction value (0 for air and 1 for water). An active absorption technique is imposed (Didier et al., 2016) by using the methodology proposed by Shäffer and Klopman (2000), based on linear shallow water theory, and has shown that it works relatively well even when used for waves outside the shallow water range.

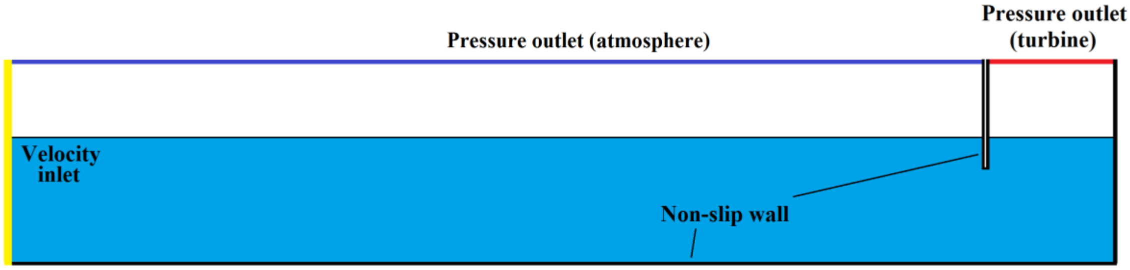

Figure 2. Boundary conditions of the numerical wave flume.

The active absorption enables also using a relative small length of the numerical flume (low computational cost), since long flume domains are typically used to increase the amount of time waves have to propagate before reflected waves start to re-reflect on the tank preventing data acquisition. The horizontal velocity component at the wave maker is corrected in real time to avoid the wave reflection. For that, it is necessary to estimate the time series of the free surface elevation, η, of the reflected wave, η_R, to be absorbed, comparing the target-free surface, η_{target}, calculated using linear wave theory, to the free surface recorded in front of the wave maker, η_{record}:

$$\eta_R = \eta_{target} - \eta_{record} \tag{4}$$

Also, the horizontal velocity component, u_1 (on the wave propagation direction), at the wavemaker has to be modified, in order to match the velocity induced by the wave to be absorbed. The velocity correction owing to absorb the reflected wave, u_{corr}, is given by

$$u_{corr} = \eta_R \left(\frac{g}{h} \right)^{1/2} \tag{5}$$

where h is the water depth. The corrected velocity at the wave maker, u_1, is obtained by:

$$u_1 = u_{target} - u_{corr} \tag{6}$$

A pressure outlet condition is imposed on the top boundary of the chamber by means of UDF (Didier et al., 2016) based on the relation between the flow rate and the pressure of a Wells turbine, given by (Torres, 2015; Sheng et al., 2013):

$$\Delta p = k_t Q \tag{7}$$

where k_t is the turbine characteristic relation that is 50 Pa s/m^3 in this study, and Δp is the pressure difference between the atmosphere and OWC chamber. Therefore, the pressure is imposed at each instant based on the flow rate of the previous instant.

Free surface level at rest (10 m depth) and atmospheric pressure on the pressure outlet are initial conditions. Previous studies have shown that wave propagation in FLUENT® is well simulated using 70 elements per wavelength in the horizontal direction, and 25 elements in the vertical direction in the region of the free surface. Consequently, the Cartesian mesh (Figure 3) is constructed with these characteristics with a refinement near the static wave maker, the wall of the coastal structures and the flume bottom (Teixeira et al., 2013; Didier et al., 2016).

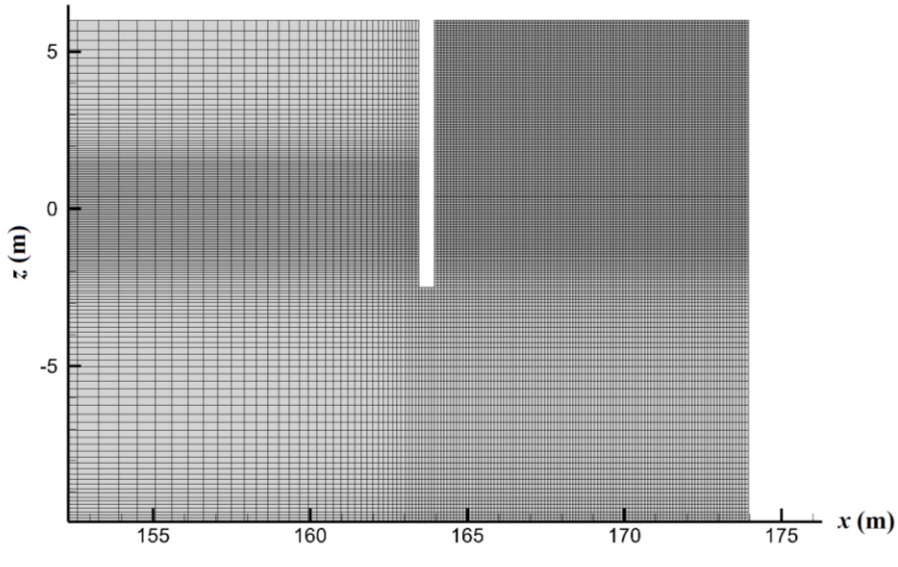

Figure 3. Cartesian finite volume mesh in detail.

2.2 Energy balance

In this study, the energy balance is evaluated based on energy chain shown in Fig. 4. By means of the law of energy conservation, the amount of wave energy entering the system will be equal to the sum of energy leaving the system plus the amount of energy absorbed in it

(Tseng et al., 2000). The absorbed energy is composed, basically, by energy losses, stored potential energy and extracted pneumatic energy.

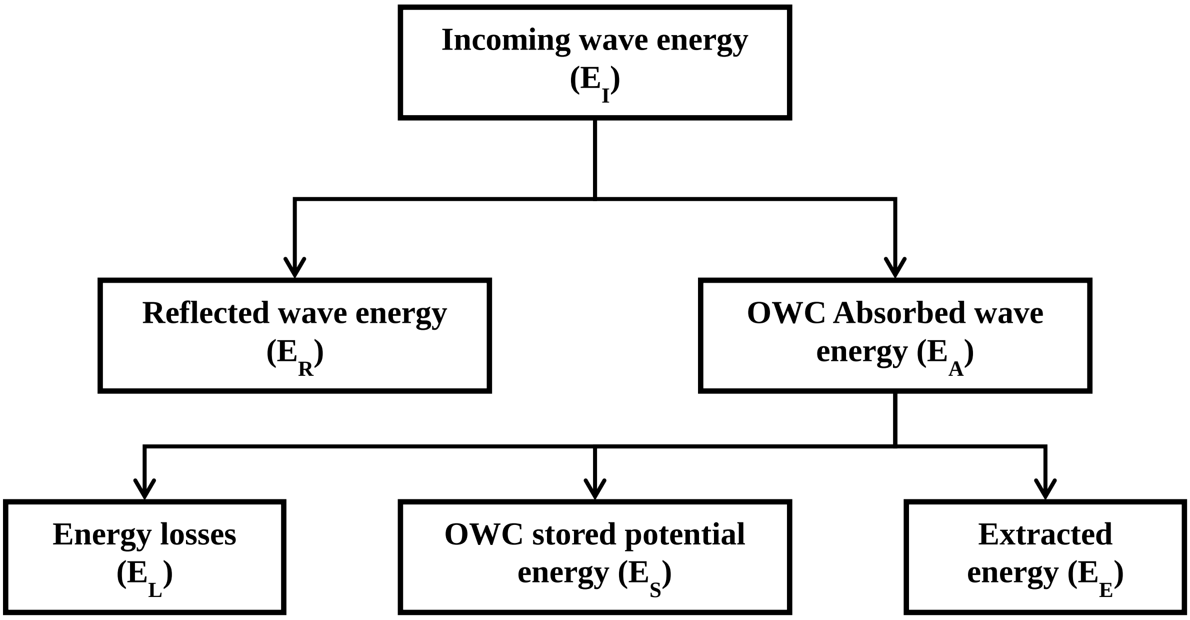

Figure 4. Energy chain in an onshore OWC.

The Incident wave energy per wave front, taking into account the linear theory (Dean and Dalrymple, 1991), is given by:

$$E_I = \frac{1}{8}\rho g H^2 L \tag{8}$$

The incident wave energy (E_I) is the sum of the reflected wave energy (E_R) and the energy absorbed by the system (E_A):

$$E_I = E_R + E_A \tag{9}$$

where energies expressed in Eq. (9) are per wave front and E_R is proportional to H_R^2 (H_R is reflected wave height) as follow (Eq. (10)):

$$E_R = \frac{1}{8}\rho g H_R^2 L \tag{10}$$

The absorbed energy (E_A) is composed by extracted pneumatic energy (E_E), stored potential energy (E_S) and energy losses (E_L) (See Fig. 4), according to the follow equation:

$$E_A = E_E + E_S + E_L \tag{11}$$

Energy losses, E_L, are due to viscous losses, turbulence and vortex formation. Experiments developed by Fleming et al. (2012) show that vortices do not participate on the water column oscillation and, consequently, they are not used to generate energy and they are considered energy losses. The stored potential energy in the oscillating waver column is expressed according to the wave linear theory (Tseng et al., 2000):

$$E_S = \frac{\rho g H_S^2 b}{16} \qquad (12)$$

where H_s is the height of the oscillating water column inside the chamber and b is the chamber width. The pneumatic energy extracted by the turbine is calculated by the expression (Elhanafi et al., 2016):

$$E_E = \int_0^T \Delta p(t) Q(t) dt \qquad (13)$$

where T is the wave period, Δp is the pressure difference between the air inside the chamber and atmosphere and Q is the volumetric flow rate caused by the free surface displacement inside the chamber.

The reflected wave height (H_R) must be determined to compute the correspondent energy (E_R) according Eq. (10). There are different methods to evaluate the reflected wave by using the Fourier transform. In this study, the method firstly proposed by Goda and Suzuki (1976), improved by Mansard and Funke (1980) for irregular waves and modified by Baquerizo (1985) is used. This method requires time series of surface elevation in three gauges and its code was implemented by using MATLAB software. These three gauges, named wp1, wp2 and wp3, are located in the wave direction at the middle of the flume, whose distances among them must be adequate to minimize numerical instabilities (Sousa et al., 2015); wp2 and wp3 are distant from wp1 in $0.1L$ and $0.27L$, respectively.

In this study, incident wave energy (E_I) and reflected wave energy (E_R) are calculated by Eq. (8) and (10), respectively. Then, absorbed energy (E_A) can be known by means of Eq. (9). Afterwards, stored potential energy (E_S) and pneumatic energy (E_E) are determined by Eqs. (12) and (13), respectively, and, finally, the energy losses (E_L) can be calculated by Eq. (11).

3. RESULTS AND DISCUSSION

Figure 5 shows the vorticity magnitude and streamlines around the OWC in nine instants during one wave period. It may be notice that vorticity magnitudes are higher in the inferior region of the front wall (maximum of 13 s^{-1}). This fact shows that there is a significant energy loss in this zone. There are vortex formations near the front wall located inside the chamber when flow has the same direction as the wave and outside the chamber when the water moves to opposite direction. There is also a vortex formation inside the chamber at $t = 2T/8$, when water column fall and, at same time, flow imposed by incident wave is into the chamber direction.

The high vorticity magnitude in the lower zone of front wall incentivated some researchers to study the influence of the shape of this part in the flow, such as Horko (2007) and Morris-Thomas et al. (2007). The methodology developed in this study to analyze the energy distribution allows evaluating the influence of the shape of this part on the device performance, quantifying viscous losses of each case.

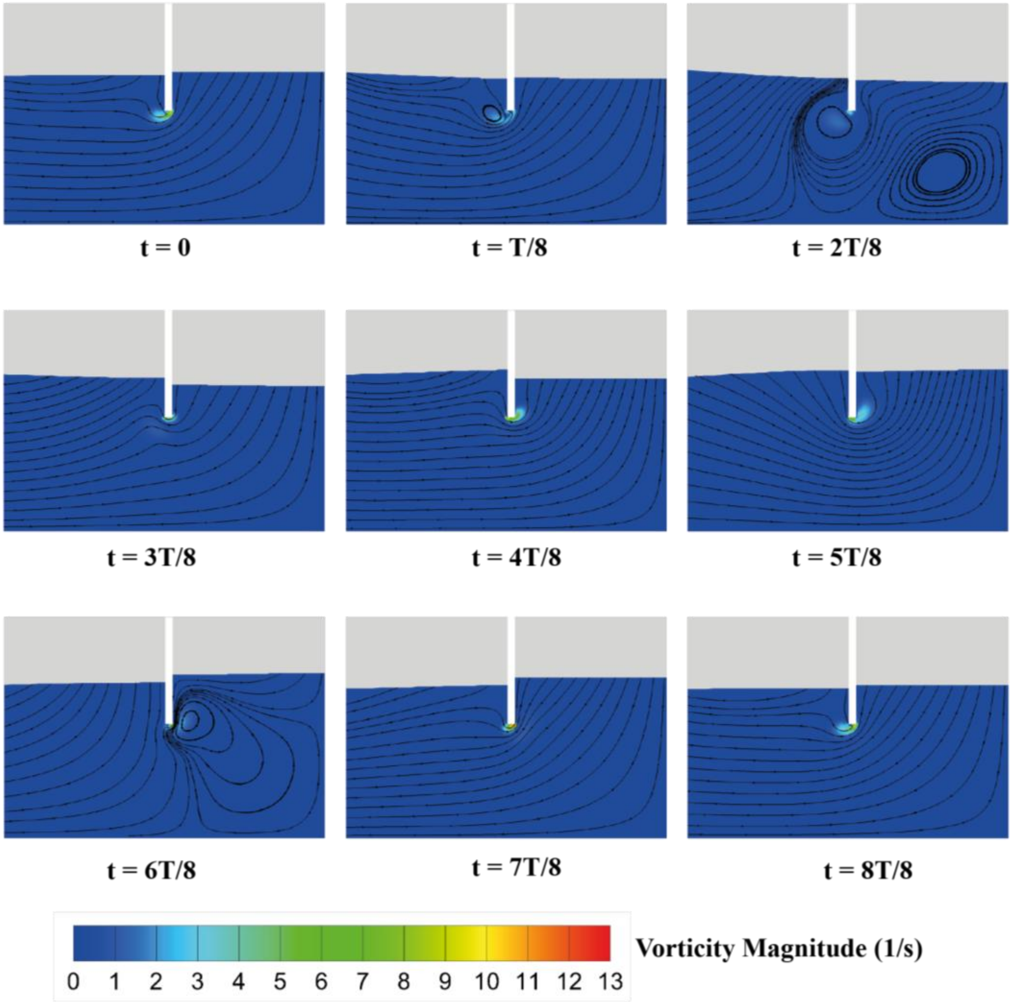

Figure 5. Vorticity magnitude and streamlines at nine instants near the OWC.

Figure 6 shows time series of free surface elevation in gauges wp1, wp2 and wp3 used to determine the wave reflection. These free surface elevations result in a reflected wave height H_R = 0.49 m.

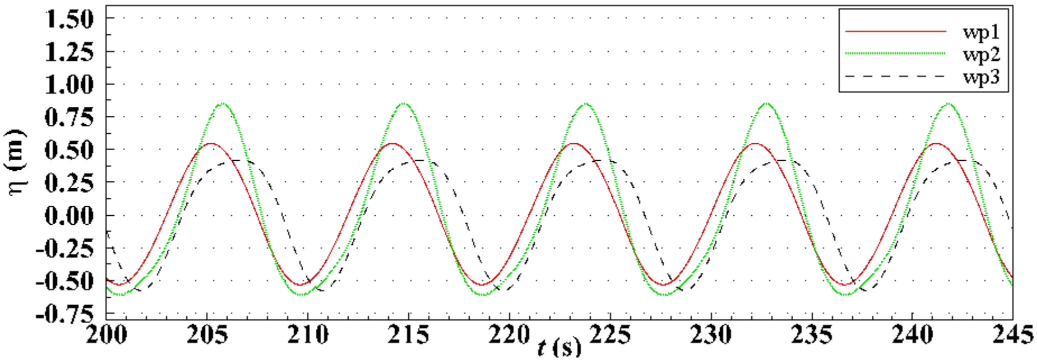

Figure 6. Time series of free surface elevation in gauges wp1, wp2 and wp3.

Figure 7 shows time series of free surface elevation and air pressure inside the chamber. The free surface elevation is the mean value of free surface elevation along the chamber length, but, in this case, they are practically uniform along the chamber length, which indicates that there is no significant sloshing. The pressure is the mean value along the chamber length in a line above the free surface. The crest is higher than the trough, that are 0.73 and 0.65 m, respectively. Figure 7 shows that the height of oscillating water column is *Hs* = 1.37 m. The pressure has an almost harmonic signal, as occurred with the free-surface elevation, and the maximum amplitude is higher than the minimum one (2500 Pa and -2300 Pa, respectively).

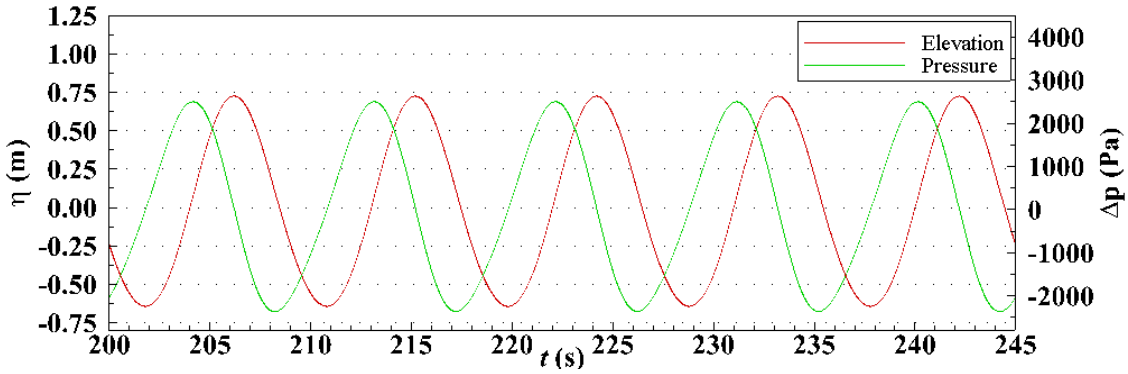

Figure 7. Time series of free surface elevation and pressure inside the OWC.

The time series of turbine flow rate is shown in Fig. 8. Considering that the air flow is incompressible, the turbine flow rate is calculated multiplying the vertical velocity of the free surface by the transversal area of the chamber that in this case is 100 m^2. The maximum amplitude (outflow) is 50 m^3/s and the minimum one (inflow) is 47 m^3/s.

The time series of pneumatic power is shown in Fig. 9, which is calculated multiplying the turbine flow rate by the pressure inside the chamber. The maximum pneumatic power is 125 kW for the maximum free surface elevation in the OWC, and 112 kW for the minimum one (mean pneumatic power of 54 kW). It can be observed that the peak during the exhalation is higher than it in the inhalation, due to the difference of amplitudes in the pressure, as expected and related by some authors (Falcão et al., 1999; Fleming et al., 2012).

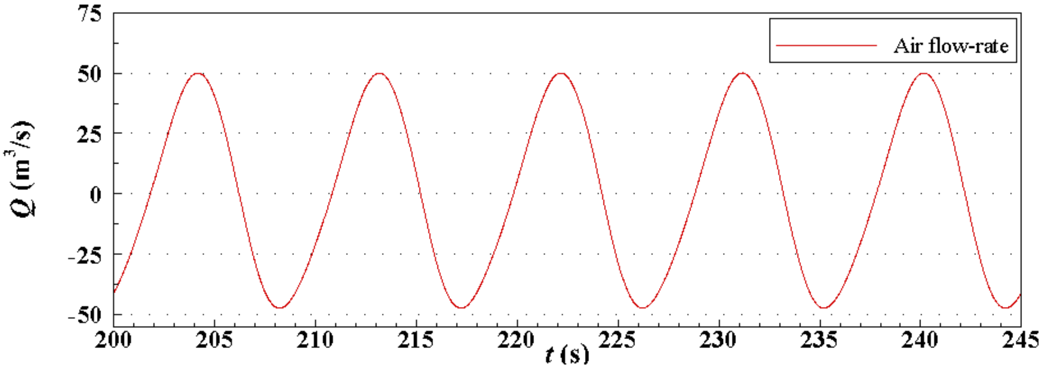

Figure 8. Time series of turbine flow rate.

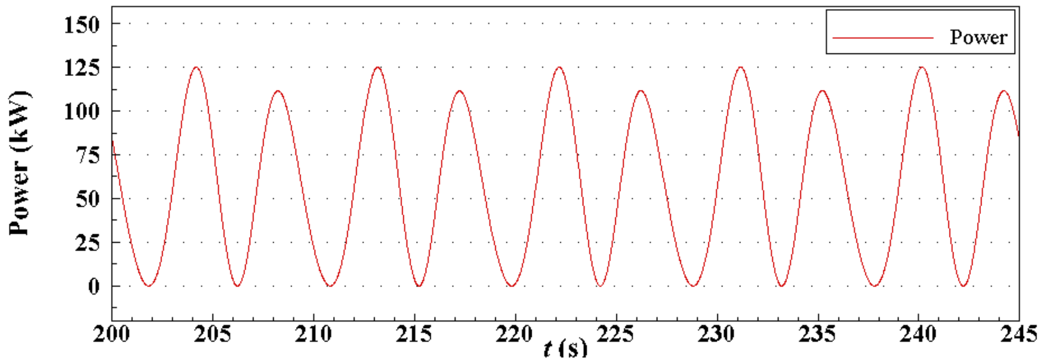

Figure 9. Time series of the pneumatic power.

Based on results measured for this case, energy distribution is quantified and can be shown in Tab. 1. Figure 10 shows the energy distribution graphically. The absorbed energy (E_A) corresponds to 74.8% of incident wave energy and the rest (25.2%) is the reflected wave energy (E_R). The pneumatic energy (E_E) is 51.8% of the incident wave energy, considered the efficiency of the device, and represents 69.2% of the absorbed energy. Energy losses (E_L) are 11.5% of the incident wave energy and 15.5% of the absorbed energy. Reflected wave energy and stored potential energy (11.5%) represent 36.7% of incident wave energy that is not used by Power Take-Off (PTO) but it is inherent in the process.

Table 1. Energy distribution obtained for the OWC.

Energy fractions	**Value (J/m)**	**% (E_I)**	**% (E_A)**
E_I	100009	100	-
E_R	25153	25.2	-
E_A	74856	74.8	100
E_S	11455	11.5	15.3
E_E	51787	51.8	69.2
E_L	11614	11.5	15.5

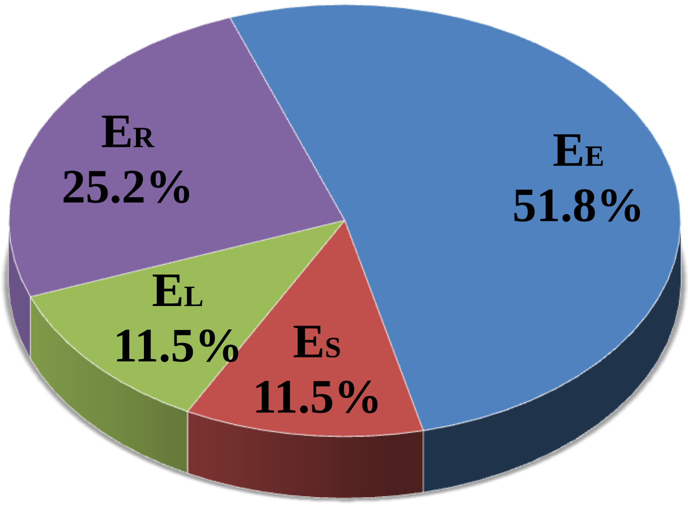

Figure10. Energy distribution.

This energy balance allows modifying the OWC design to decrease energies that do not contribute to the efficiency of the device, e.g., devices with a sloped frontal wall, such as in LIMPET plant can diminish viscous losses because of fewer obstacles to the flow. Besides, the reflected wave energy is modified, mainly because of run-up and run-down phenomena on the front wall that alter completely the wave-structure interaction.

4. CONCLUSIONS

Analysis of the energy distribution in an onshore OWC device, at the end of a flume 10 m deep, subjected to a regular wave with a wave period of 9 s and a wave height of 1m, was carried out. FLUENT® RANS-VOF model was used and methodologies to consider a Wells turbine, with turbine characteristic relation equal to 50 Pa s/m^3, and wave generation with active absorption, were employed. The geometry of the OWC, 10 m long and 10 m wide, is similar to that of the Pico plant, Portugal. A model to calculate the reflected wave height, based on methodology developed by Mansard and Funke (1980), was applied and a reflected wave height of 0.49 m was obtained.

Vorticity magnitude distribution showed that higher values occur near the lower part of the front wall, which indicates that significant viscous losses, that are a portion of energy losses, are located in this zone. The time series of pneumatic power showed that the maximum amplitude for exhalation was higher (125 kW) than inhalation one (112 kW). It occurs because differences of inflow and outflow of the water, due to effects of wave structure interactions, cause positive amplitudes higher than negative ones in both free surface elevation and pressure inside the chamber.

The absorbed energy corresponded to 74.8% of the incident wave energy and the rest (25.2%) was reflected wave energy. The pneumatic energy is a part of the absorbed energy and it was 51.8% of the incident wave energy that corresponds to the device efficiency. Energy losses represented 11.5% of the incident wave energy that, in this case, was equal to the stored potential energy.

This analysis allows understanding the wave energy distribution due to the incidence of waves on an OWC device. Therefore, different conceptions can be proposed to decrease energy losses during the wave energy extraction process. Energy losses due to turbulence, wave breaking and, mainly, viscous losses, as well as wave reflected energy, can be compared between different conceptions of OWC to search the solution with better device performance for a specific regional wave climate.

Acknowledgements

The first author acknowledges the support of CAPES for the post-graduate scholarship and Universidade Federal do Rio Grande - FURG through PROPESP, for the resources granted which allowed for participation in the congress.

REFERENCES

Baquerizo, A., 1995. *Reflexión del oleaje en playas. Métodos de evaluación y de predicción***.** PhD thesis, Universidad de Cantabria.

Cruz, J. 2008. The Wave Energy Resource. In Barstow, S., Mϕrk, G. & Cruz, J., eds, *Ocean Wave Energy: Current Status and Future Perspectives*, PP. 93–132. Springer-Verlag.

Dean, R. G., & Dalrymple, R. A., 1991. Water wave mechanics for engineers and scientists. *World Scientific.*

Didier, E., Teixeira, P.R.F., & Neves, M.G., 2016. A 3D Numerical Wave Tank for Coastal Engineering Studies. *In Defect and Diffusion Forum*, vol. 372, pp. 1–10.

Elhanafi, A., Fleming, A., Macfarlane, G., & Leong, Z., 2016. Numerical energy balance analysis for an onshore oscillating water column - wave energy converter. *Energy*, vol. 116, pp. 539–557.

Falcão, A. F. de O., 2010. Wave energy utilization: A review of the technologies. *Renewable & Sustainable Energy,* vol. 14, n. 3, pp. 899–918.

Falcão, A. F. de O., 2000. The shoreline OWC wave Power plant the Azores. In Østergaard, I. & Iversen, S., eds, *Proceedings of the Fourth European Wave Energy Conference (EWTEC-4).*

Falcão, A. F. de O. & Justino, P. A. P., 1999. OWC wave energy devices with air flow control, *Ocean Engineering*, vol. 26, pp. 1275–1295.

Fleming, A., Penesis, I., Macfarlane, G., Bose, N., & Denniss, T., 2012. Energy balance analysis for an oscillating water column wave energy converter. *Ocean Engineering,* vol. 54, pp. 26–33.

Folley, M., Whittaker, T., 2002. Identification of non-linear flow characteristics of the LIMPET shoreline OWC. In S. Chung, J.S., Sayed, M., Kashiwagi, M., Setoguchi, T., & Hong, S.W., eds, *Proceedings of The Twelfth International Offshore and Polar Engineering Conference*, pp. 541–546.

Ghosh, T. K., & Prelas, M. A., 2011. *Energy Resources and Systems. Volume 2: Renewable Resources*. Springer.

Goda, Y. & Suzuki, Y., 1976, Estimation of Incident and Reflected Waves in Random Wave Experiments. *Proceedings of the 15th Coastal Engineering Conference*.

Horko, M., 2007. *CFD Optimisation of an oscillating water column wave energy converter.* Degree of master of engineering scince thesis, University of Western Australia.

Lewis, A., Estefen, S., Huckerby, J., Musial, W., Pontes, T., & Torres-Martinez, J., 2011. *In* Edenhofer, O., Pichs-Madruga, R., Sokona, Y., Seyboth, K., Matschoss, P., Kadner, S., Zwickel, T., Eickemeier, P., Hansen, G., Schlömer, S., & Stechow, C. von, eds., *Ocean*

Energy: IPCC Special Report on Renewable Energy Sources and Climate Change Mitigation, Cambridge University Press, Cambridge, United Kingdom and New York, NY, USA.

Mansard, E. P. D. & Funke, E. R, 1980. The Measurement of Incident and Reflected Spectra Using a Least Squares Method. *Coastal Engineering*, vol. 4, pp. 154–174.

Morris-Thomas, M. T., Irvin, R. J., & Thiagarajan, K. P., 2007. An investigation into the hydrodynamic efficiency of an oscillating water column. *Journal of Offshore Mechanics and Arctic Engineering*, vol. 129, pp. 273–278.

Schäffer, H. A., & Klopman, G., 2000. Review of multidirectional active wave absorption methods. *Journal of waterway, port, coastal, and ocean engineering,* vol. 126, n. 2, pp. 88–97.

Sheng, W., Alcorn, R., & Lewis, A., 2013. On thermodynamics in the primary power conversion of oscillating water column wave energy converters. *Journal of Renewable and Sustainable Energy,* vol. 5, n.2.

Sousa, G. A. C. F., Neves, M. G., & Capitão, R., 2011. Separação de agitação incidente e reflectida: testes comparativos. *7ªs Jornadas Portuguesas de Engenharia Costeira e Portuária, AIPCN-PIANC*.

Teixeira, P. R. F., Davyt, D .P., Didier, E., & Ramalhais, R., 2013. Numerical simulation of an oscillating water column device using a code based on Navier-Stokes equations. *Energy*, vol. 61, n. 1, pp. 513–530.

Tseng, R.S., Wu, R. H., & Huang, C.C., 2000. Model study of a shoreline wave-power system. *Ocean Engineering*, vol. 27, pp. 801–821.

Torre-Enciso, Y., Ortubia, I., López de Aguileta, L.I., & Marqués, J., 2009. Mutriku Wave Power Plant: from the thinking out to the reality. *In Proceedings of the 8th European Wave and Tidal Energy Conference (EWTEC-8),* pp. 319–329.

Torres, F. R., 2015. Método numérico simplificado para determinação das curvas de potência mecânica de turbina wells instalada em dispositivo para captação da energia da sondas do tipo coluna de água oscilante sob incidência de ondas monocromáticas. Degree of master thesis, Universidade Federal do Rio Grande – FURG.